# Application of Resistance Curves to Residual Strength Prediction

**M. M. RATWANI**

**D. P. WILHEM**

Senior Technical Specialist,
Northrop, Corp.,
Hawthorne, Calif.

*A resistance curve approach to predicting residual strength of thin-skin structures, under plane stress type fracture, is discussed. Use is made of material resistance obtained in terms of crack extension as a function of the square root of $J(\sqrt{J_R})$. Prediction has been made of the residual strength of two types of structures, namely stiffened aircraft panels and thin-wall cylindrical pressure vessels. Elastic-plastic analysis based on a Dugdale-type strip plastic zone is used in the residual strength prediction. The analytical results are compared with available experimental data.*

## Introduction

In recent years, considerable work has been done in developing resistance curves of various materials. Standard tests have been established by ASTM [1][1] to obtain the resistance curves of metallic materials using crackline wedge-loaded (CLWL) specimens. The introduction of the CLWL specimen, first suggested by Anderson [2] and developed by Heyer and McCabe [3], has made it possible to track the stable crack growth over large crack extension ranges. The crack growth data in terms of linear elastic fracture mechanics have been discussed in references [3 and 4]. The crack growth resistance of materials accounting for the elastic-plastic behavior of materials has been recently reported by Ratwani and Wilhem [5, 6]. The crack growth resistance has been represented in terms of the $J$ integral [7] in these studies.

The use of the resistance curve approach to structural application has attracted very little attention. Creager and Liu [8] used the resistance curve approach to predict the residual strength of simple strap reinforced sheet panels. However, the use of the resistance curve was restricted due to the lack of a suitable elastic-plastic analysis. Ratwani and Wilhem [5, 9] carried out a systematic elastic-plastic analysis of aircraft structures in order to develop a technique to predict residual strength for plane stress type fractures. Their investigations showed that the $J$ integral represents a very suitable parameter to account for the plasticity ahead of a crack tip. $J$ integral values in a cracked structure along with the $\sqrt{J}_R$ resistance curve of the material represents a very convenient way of predicting failure in a structure. The residual strength prediction technique and its application to stiffened aircraft panels and thin-walled pressure vessels are discussed in the following paragraphs.

## Residual Strength Prediction Technique

A failure criterion based on crack growth resistance was first introduced by Irwin [10], and an extensive discussion on this has been given by Krafft, et al [11]. They suggested that a crack will grow in a stable fashion when the increase in resistance with crack extension is greater than the increase in applied stress intensity. If these conditions are not met, unstable fast fracture will occur. Thus, fast fracture will occur when

$$K = R, \text{ and } \frac{\partial K}{\partial a} \geq \frac{\partial R}{\partial a}$$

This method of employing stress intensity factors along with the material $K_R$ curve has several disadvantages associated with estimates of crack tip plasticity [12]. The concept can be extended to incorporate plasticity effects by using the $J$-Integral in place of the stress intensity factor $K$. The use of $J$ has several advantages, as discussed in reference [12]. The residual strength prediction procedures involves the following steps:

1. Obtain the $\sqrt{J}_R$ curve for the skin material of the structure using a suitable specimen (e.g., crackline wedge loaded or center-crack tension) [5, 6].
2. Obtain $J$ values for the structure of interest at various crack lengths and applied stress using a suitable model of plasticity at the crack tip [5, 13, 14] (e.g., Dugdale model [15]).
3. Determine the point of instability from the $\sqrt{J}$ curves of the structure and the $\sqrt{J}_R$ curves of the material as shown in Fig. 1.

Curves representing the square root of $J$ versus crack length are plotted for various applied stresses. The $\sqrt{J}_R$ resistance

[1]Numbers in brackets designate References at end of paper.

Contributed by the Materials Division for publication in the JOURNAL OF ENGINEERING MATERIALS AND TECHNOLOGY. Manuscript received by the Materials Division, July 1977; revised manuscript received November 2, 1977.

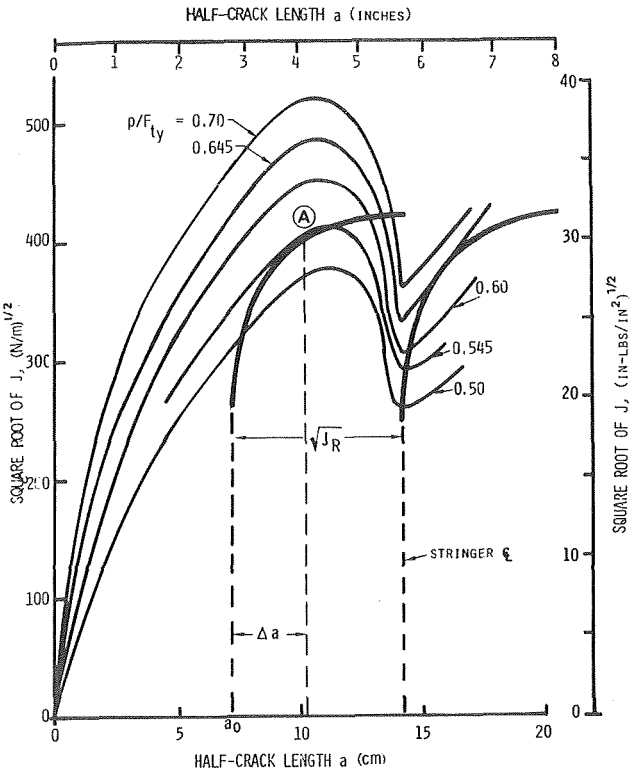


**Fig. 1 Residual strength prediction plot for an all-aluminum panel**

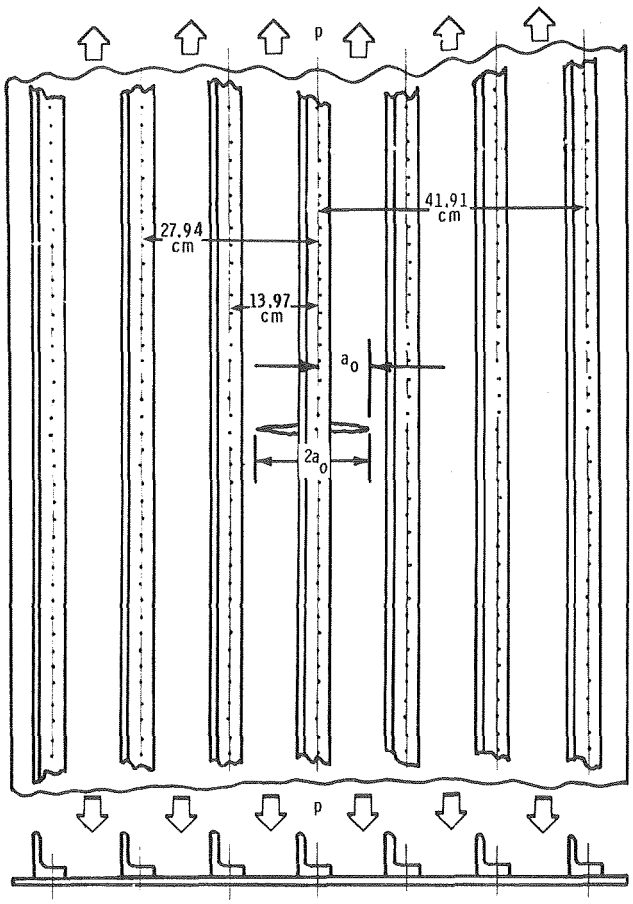


**Fig. 2 Geometry of test panel**

curve is superimposed on the diagram at some physical crack length under consideration, say $a_0$. The corresponding failure stress is given by the point of tangency between the $\sqrt{J_R}$ curve and the $\sqrt{J}$ curve at point A, as shown in Fig. 1. The fracture is associated with a slow tear of the amount $\Delta a$, to point A.

## Application of Resistance Curves to Residual Strength Prediction of Aircraft Structures

In a stiffened aircraft panel, the failure may be due to a stringer failure (stringer critical case) or skin failure (skin critical case). These two types of failure are discussed in references [5, 9, 16, and 17]. The failure due to skin critical cases is predictable by using the technique just discussed. In using this technique, an important consideration is the type of elastic-plastic analysis to be used. Two common types of elastic-plastic analyses involve 1) the Dugdale-type strip plastic zone model (ahead of the crack tip), or 2) the Prandtl-Reuss material behavior. It was shown in references [5 and 9] that for stiffened panel geometries, the $\sqrt{J}$ values obtained assuming the Dugdale-type material behavior approached those obtained by the Prandtl-Reuss behavior at greatly reduced effort and cost.

## Residual Strength Prediction of an All-Aluminum Panel

Consider the wing panel geometry shown in Fig. 2, where the skin is 1.60 mm (0.064-in.) thick 7075-T73, and the stiffeners are 7075-T6 angle extrusions. The elastic-plastic analysis of this panel was carried out for various crack lengths, assuming a Dugdale type of plastic zone, using the Bueckner-Hayes approach [5, 14]. For Dugdale-type behavior, the relation between crack opening displacement and the $J$-integral is given by

$$J = \delta F_{ty}$$

where $\delta$ is the crack opening at the physical crack tip and $F_{ty}$, the skin material yield stress. Strictly, $F_{ty}$ is the flow stress of an ideally plastic material. The tensile yield strength might be considerably lower than the best estimate for a work hardening elastoplastic material.

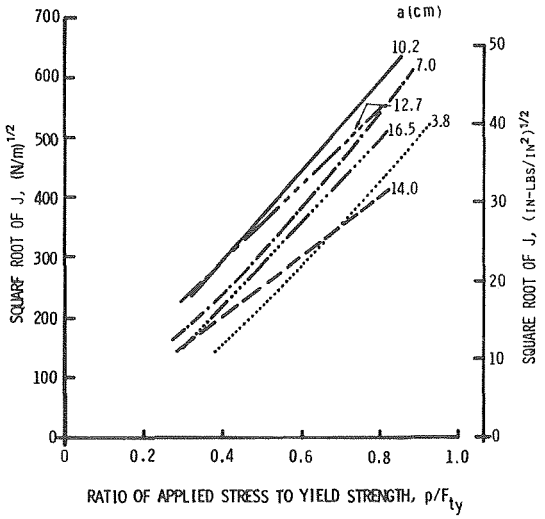


**Fig. 3 Square root of $J$ as a function of applied stress for varying crack lengths—intact stringer case**

The values of $J$ are obtained from the computed crack openings for various applied stresses. The plot of $\sqrt{J}$ versus the ratio of applied stress to yield stress $(p/F_{ty})$ at various crack lengths is shown in Fig. 3. In Fig. 1, these values are cross-plotted to show the variation of the square root $J$ with crack

length at various applied stresses. To determine the residual strength of the panel at any half-crack length (for example 7.05 cm), the resistance curve of the skin material (7075-T73) is overlayed at that crack length, as shown in Fig. 1. From this figure, the resistance curve of the material is tangential to the $\sqrt{J}$ versus the $a$ curve of the panel at an applied stress of $p/F_{ty} = 0.545$. Thus, the first point of crack instability occurs after slow crack growth at this stress, and the crack starts a rapid advance. However, from Fig. 1, it is noted that at half-crack length of 11.3 cm (4.45 in.), the $\sqrt{J}$ curve for the panel drops below the resistance curve of the material. Thus, beyond this point, the resistance of the material is higher than the $\sqrt{J}$ developed in the stressed panel, hence the running crack will become arrested. The crack would most likely be arrested at the fastener hole in the panel where the stringer is connected to the skin. The resistance curve of the skin material is now replotted at a half-crack length of 13.97 cm (5.5 in., distance from the panel center line to the center line of the stringer), where the crack became arrested. For this crack length, the $\sqrt{J}$ curve of the panel becomes tangential to the resistance curve at an applied stress of $p/F_{ty} = 0.645$. Hence, the crack instability occurs at that stress and the crack starts running catastrophically. Beyond this point of instability, the $\sqrt{J}$ values in the panel are higher than the resistance curve of the skin material. therefore no possibility exists for crack arrest. The $\sqrt{J}$ curve of the panel will continue to rise under increasing load until the influence of the next stringer on panel stress is felt 27.94 cm (11 in.) from the center line of the panel and $\sqrt{J}$ value will once again have a decreasing trend and reach a second minima at that point. From the trend of the $\sqrt{J}$ curve in Fig. 1, it is evident that at an applied stress of $p/F_{ty} = 0.645$, the $\sqrt{J}$ value of the panel will be higher than for any half-crack length beyond 19.05 cm (7.5 in.). Therefore, no crack arrest is possible at the second stringer, i.e., 27.94 cm (11 in.) from the center line of the crack, under increasing load conditions.

The panel analyzed above ($a_0 = 7.05$ cm (2.775 in.)) was tested to failure. Slow tear in this panel started at a load of 0.267 MN (60 kips), which corresponds to $p/F_{ty} = 0.32$ ($F_{ty} = 424.1$ MN/m² or 61.5 ksi). At this applied load, slow tear on each crack tip was about 0.51 mm (0.02 in.). The first point of instability (rapid crack extension) occurred after an applied load of 0.267 MN (60 kips) and before a load of 0.497 MN (111.7 kips). At 0.497 MN (111.7 kips), the crack had already reached the angle stiffeners and became arrested. From theory, the first point of instability is at an applied stress of 0.545 $F_{ty}$, or a load of 0.463 MN (104 kips) (see Fig. 1). After the crack had torn to the angle stiffeners, the panel was able to take a load of 0.497 MN (111.7 kips) without any further slow tear. At an applied load of 0.497 MN (111.7 kips); i.e., $p/F_{ty} = 0.58$, the slow tear from Fig. 1 is approximately 1.27 mm (0.05 in.). This is less than the radius of the rivet hole connecting the stringer to the skin in Fig. 2.

The measured failure load of the panel was 0.516 MN (116.1 kips). The predicted failure is $p/F_{ty} = 0.645$, or a panel load of 0.549 MN (123.4 kips). This predicted failure load is within 6.3 percent of the measured failure load for the panel.

## Residual Strength Prediction of an All-Titanium Panel

The residual strength prediction technique was applied to an all titanium panel similar to the panel of Fig. 2. The skin in this case was 1.47 mm (0.058 in.) thick Beta mill annealed Ti-6Al-4V. The angles were made from annealed Ti-6Al-6V-2Sn. The overall skin width was 97.8 cm (38.5 in.), with a panel length of approximately 229 cm (90 in.).

The $\sqrt{J}$ versus crack length plots for several applied stresses similar to those of Fig. 1, were obtained for various crack lengths using the procedure discussed previously. The $\sqrt{J_R}$ versus $\Delta a_{PHY}$ resistance curve of the Beta mill annealed Ti-6Al-4V skin material plotted at a physical half-crack length of 7.19 cm (2.83 in.) is superimposed on the plot. The resistance curve of the material is tangential to the $\sqrt{J}$ curve of the panel at an applied stress of $p/F_{ty} = 0.66$, where the first point of crack instability occurs after an initial period of slow crack growth. Immediately after the point of instability, the $\sqrt{J}$ curve for the panel drops below the resistance curve of the material. The crack will become arrested where the next stringer (angle) is connected to the skin. The resistance curve of the material is now replotted at a half-crack length of 13.97 cm (5.5 in., distance from center line of the stringer to the panel center line) where the crack became arrested. For this crack length, the $\sqrt{J}$ curve of the panel becomes tangent to the resistance curve at an applied stress of $p/F_{ty} = 0.69$. Hence the second point of crack instability occurs at this stress and the crack runs catastrophically.

The actual failure stress of the tested panel was 527. MN/m² (76.45 ksi) compared to a predicted failure stress of 543.9 MN/m² (78.86 ksi, corresponding to $F_{ty} = 788.3$ MN/m², 114.3 ksi). The predicted and actual failure stress of various panels tested in references [5 and 9] are given in Table 1. It may be noted that most of the predicted values are higher than those observed.

## Application of the Resistance Curve Approach to Residual Strength Prediction of Cracked Pressure Vessels

Consider a thin-walled, cylindrical shell with a longitudinal crack as shown in Fig. 4(*a*). The elastic analysis of such a structure has been carried out by several investigators [18–20]. The analysis of this study was carried out using the eighth-order shell theory. The solution of the problem was reduced to dual integral equations which were solved numerically. The stress intensity factors have been obtained for various shell parameter values $\lambda$ given by

**Table 1 Comparison of predicted and measured strengths of various panel geometries**

| Type of panel | Half-crack length "$a$" cm (in.) | Residual strength MN/m² (ksi) Predicted | Residual strength MN/m² (ksi) Measured | Percentage difference |
|---|---|---|---|---|
| Riveted zee stiffeners with lands | 5.42 (2.126) | 276.1 (40.05) | 256.8 (37.25) | + 7.50 |
| Bolted zee stiffeners with lands | 5.40 (2.126) | 276.1 (40.05) | 250.9 (36.39) | +10.04 |
| Adhesively bonded zee stiffeners with lands | 5.20 (2.047) | 302.0 (43.80) | 289.8 (42.03) | + 4.21 |
| Riveted zee stiffeners with lands | 11.20 (4.409) | 189.6 (27.50) | 179.1 (25.98) | + 5.86 |
| Bolted zee stiffeners with lands | 11.75 (4.626) | 186.2 (27.00) | 182.1 (26.41) | + 2.25 |
| Adhesively bonded zee stiffeners with lands | 10.70 (4.213) | 198.6 (28.80) | 199.8 (28.98) | − 0.60 |
| Intact stringer - thin skin | 7.05 (2.776) | 274.0 (39.73) | 257.7 (37.37) | + 6.32 |
| Broken stringer - thin skin | 7.00 (2.756) | 237.0 (34.36) | 238.0 (34.51) | − 0.42 |
| All-titanium panel | 7.20 (2.835) | 543.7 (78.86) | 527.1 (76.45) | + 3.15 |
| Aluminum panel thick skin | 11.20 (4.409) | 255.3 (37.02) | 267.4 (38.78) | − 4.74 |

$$\lambda = [12(1 - \nu^2)]^{1/4} \frac{a}{\sqrt{Rh}}$$

where

$\nu$ = Poisson's ratio

$a$ = half-crack length

$R$ = radius of shell

$h$ = wall thickness of the shell.

The elastic-plastic analysis of the cylindrical shell with an axial crack (Fig. 4(*b*)) was treated by Erdogan and Ratwani [21], assuming a Dugdale-type plastic zone ahead of the crack. The elastic-plastic analysis is complicated due to the fact that in shell structures there are bending, as well as extensional stress singularities. It is assumed that in the plastic zone an unknown normal force $N$, and bending moment $M$ per unit length are acting as noted in Fig. 4(*b*)). The three unknowns, $N$, $M$, and the size of the plastic zone are obtained from the conditions that extensional and bending stress singularities vanish at the fictitious crack tip ($a_p$ of Fig. 4(*b*)). In addition, $N$ and $M$ satisfy the following yield criteria

$$\frac{N}{hF_{ty}} + \frac{1}{2}\left|\frac{6M}{h^2F_{ty}}\right| = 1,$$

where $F_{ty}$ is the yield stress of the shell material. These three conditions result in highly nonlinear equations that were solved numerically in reference [21]. Plastic zone size and crack opening displacement $\delta$ (COD) have been obtained for various shell parameters $\lambda$ [21]. A typical plot of $\delta$ (COD) versus $N_0/hF_{ty}$ (where $N_0$ is the membrane load perpendicular to the crack) for various values of $\lambda$, is shown in Fig. 5. The relation between the $J$ integral and $\delta$ (COD) for the Dugdale-type plastic zone is as noted previously, $J = \delta F_{ty}$. From the $\delta$ (COD) versus $N_0/hF_{ty}$ curves of Fig. 5, a plot between $\sqrt{J}$ and crack length, $a$, can be obtained at various applied stresses by cross-plotting if the shell geometry ($R$ and $h$) is known. A typical plot for a 2014-T6 aluminum shell with a radius of 7.14 cm (2.81 in.) and a wall thickness of 1.52 mm (0.06 in.), is shown in Fig. 6. Note that each $\sqrt{J}$ versus, $a$, curve increases monotonically with crack length; there are no extrema in the absence of stiffening members, hence there is no possibility of crack arrest. To evaluate the residual strength of this pressure vessel, the $R$ curve of 1.52 mm (0.06 in.) thick, 2014-T6 aluminum at 77K (−320F) given in reference [4], is plotted at the desired crack length(s) in Fig. 6. It is seen that for $a$ = 5.08 mm (0.2 in.), the point of instability is reached at $N_0/hF_{ty}$ = 0.5. Similarly, points of instability can be obtained for other crack lengths, as shown. For example, with $a$ = 17.78 mm (0.7 in.), $N_0/hF_{ty}$ = 0.16. Thus, the load-carrying capacity or residual strength of the shell is obtained for various crack lengths, as

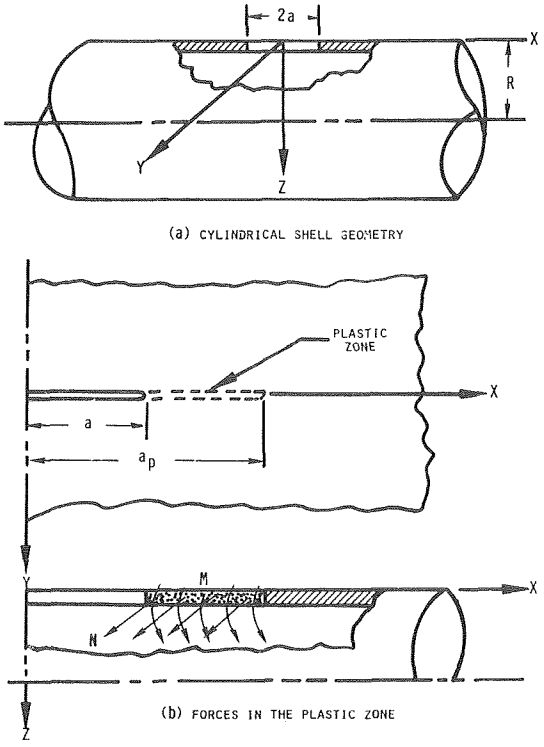


Fig. 4 Through-crack geometry in a pressurized shell

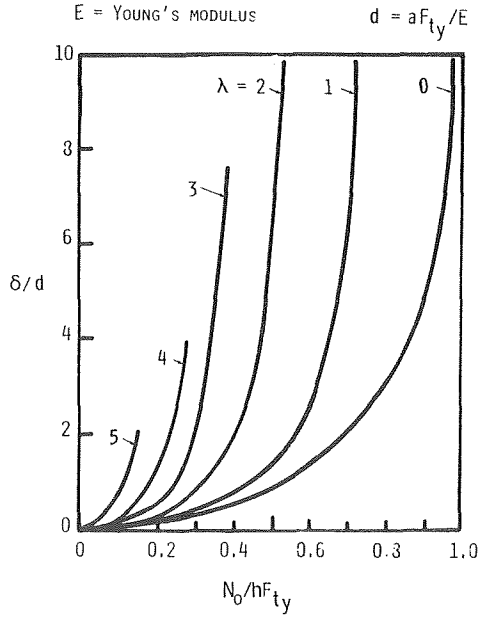


Fig. 5 Crack opening displacement (at $X = a$) for a pressurized cylindrical shell with an axial crack

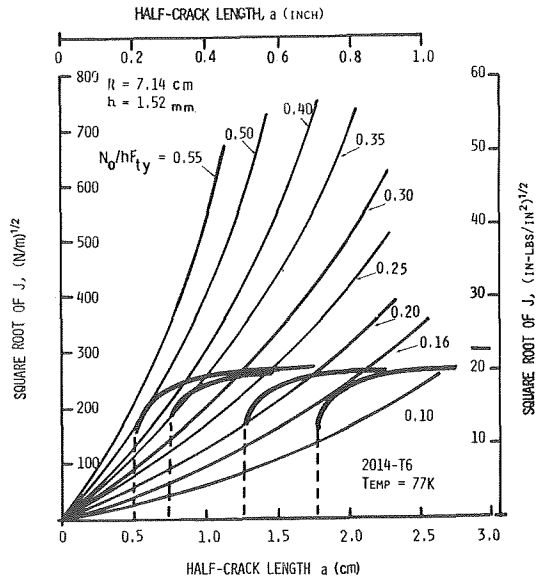


Fig. 6 Failure prediction with $\sqrt{J_R}$ curve for pressurized cylindrical shell with an axial crack

plotted in Fig. 7. Also indicated, are the experimental failure loads of the pressure vessels obtained from reference [22]. Correlation between analytical and experimental results is remarkably good.

The stable crack growth prior to the point of instability, can also be obtained. Using the data of Fig. 6, a plot of crack extension versus crack length can be constructed, as shown in Fig. 8. The experimental results from reference [22] are also noted. It is seen that the trend of experimental data is similar to that derived from the analytical predictions. However, the magnitude differs significantly. The experimental crack extension data show a very wide scatter in data, perhaps due to lack of suitable techniques to measure crack extension.

The plots of $\sqrt{J}$ versus half-crack length, $a$, similar to Fig. 6, for a shell with a geometry of $R$ = 7.14 cm (2.81 in.), and $h$ = 1.52 mm (0.06 in.), tested at 20K (−423F) were obtained, as described earlier. Assuming the resistance curve at 20K (−423F) to be similar to the one at 77K (−320F), the resistance curve of the material [4] at 77K (−320F) was plotted at various crack lengths to obtain the failure load. The load-carrying capacity of the shell for various assumed crack lengths is shown in Fig. 9, which also indicates the experimental results of reference [22]. The correlation of analytical and experimental results is good.

It may be noted that the shell analysis presented here is based on the assumption that the wall thickness-to-radius ($h/R$) ratio is sufficiently small to allow the cylindrical vessel to be treated as a shallow shell. The analysis may be used up to a $h/R$ equal to about 0.1 [20].

## Conclusions

A resistance curve approach can be successfully used to predict the residual strength of thin-skin structures with considerable amounts of crack tip plasticity and slow tear. By the use of the $\sqrt{J}$ and $\sqrt{J_R}$ curves, it is also possible to predict stable crack growth and crack arrest.

## Acknowledgments

Sponsorship by the Air Force Flight Dynamics Laboratory for the first part of this research project (stiffened panels) is acknowledged. The secretarial assistance of Pat Barnes is also acknowledged.

## References

1 "Tentative Recommended Practice fro R-Curve Determination," E561-76T, American Society for Testing and Materials, Annual Book of ASTM Standards, Part 10, 1976, pp. 539–557.

2 Anderson, W. E., "On $K_{Ic}$ et Sequentes," Note presented to ASTM Committee E24, Mar. 1968.

3 Heyer, R. H., and McCabe, D. E., "Plane-Stress Fracture Toughness Testing Using a Crack-Line-Loaded Specimen," *Engineering Fracture Mechanics*, EFMEA, Vol. 4, pp. 393–412.

4 Heyer, R. H., and McCabe, D. E., "Crack Growth Resistance in Plane-Stress Fracture Testing," *Engineering Fracture Mechanics*, EFMEA, Vol. 4, pp. 413–430.

5 Ratwani, M. M., and Wilhem, D. P., "Development and Evaluation of Methods of Plane Stress Fracture Analysis, Part II, Volume I, A Technique for Predicting Residual Strength of Structure," AFFDL-TR-73-42, Part II, Vol. I, Apr. 1975.

6 Wilhem, D. P., Ratwani, M. M., and Zielsdorff, G. F., "A J-Integral Approach to Crack Resistance for Aluminum, Steel and Titanium Alloys," ASME JOURNAL OF ENGINEERING MATERIALS AND TECHNOLOGY, Vol. 99, Apr. 1977.

7 Rice, J. R., "A Path Independent Integral and Approximate Analysis of Strain Concentration by Notches and Cracks,"

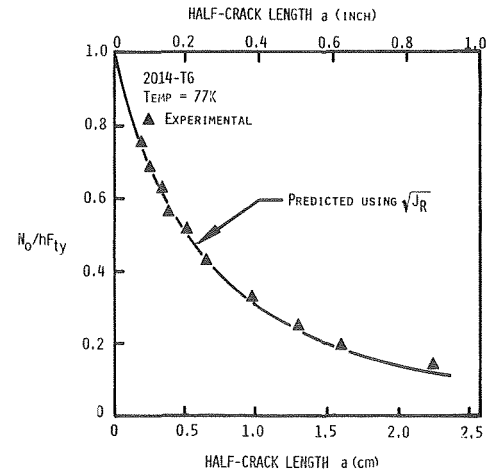


**Fig. 7 Normalized failure stress as a function of crack length for pressurized cylindrical shell with an axial crack 77K (−320F)**

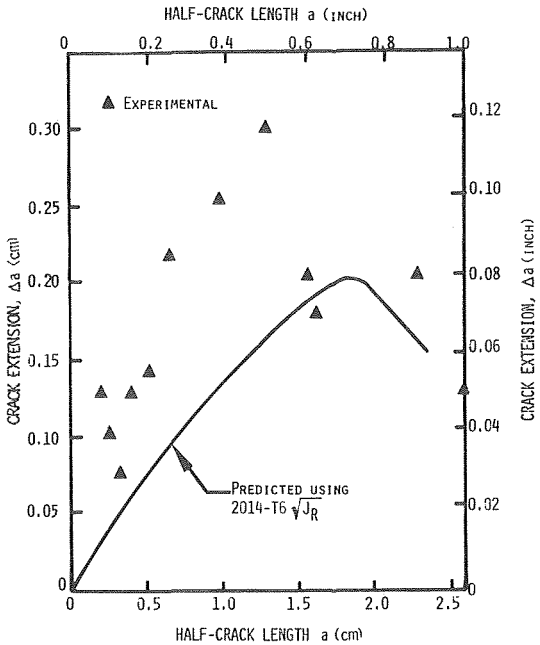


**Fig. 8 Crack extension versus crack length for pressurized cylindrical shell 77K (−320F)**

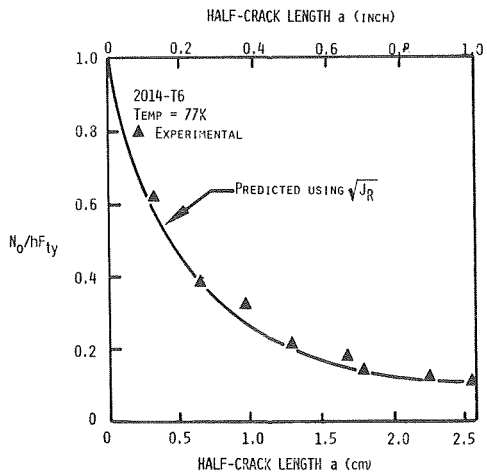


**Fig. 9 Normalized failure stress as a function of crack length for pressurized cylindrical shell with an axial crack 20K (−423F)**

*Journal of Applied Mechanics*, TRANS. ASME, June 1968, pp. 379–386.

8 Creager, M., and Liu, A. F., "The Effect of Reinforcements on the Slow Stable Tear and Catastrophic Failure of Thin Metal Sheet," AIAA Paper No. 71–113, Jan. 1971.

9 Ratwani, M. M., and Wilhem, D. P., "Development and Evaluation of Method of Plane Stress Fracture Analysis—Part III, Application of Residual Strength Prediction Technique to Complex Aircraft Structure," AFFDL-TR-73-42, Part III, Oct. 1975.

10 Irwin, G. R., "Fracture Testing of High Strength Sheet Materials under Conditions Appropriate for Stress Analysis," Report 5486, U. S. Naval Research Laboratory, July 27, 1960.

11 Krafft, J. M., et al., "Effect of Dimensions on Fast Fracture Instability of Notched Sheets," in *Proceedings of the Crack Propagation Symposium*, College of Aeronautics, Vol. 1, Cranfield, England, 1961.

12 Wilhem, D. P., "An Improved Technique for Residual Strength Prediction—A Modified Crack Growth Resistance Approach," *Proceedings of an International Conference on Prospects of Fracture Mechanics*, Delft University of Technology, The Netherlands, G. C. Sih, H. C. Van Elst, and D. Broek, Editors, June 1974, pp. 389–404.

13 Hayes, D. J., "Some Applications of Elastic-Plastic Analysis to Fracture Mechanics," PhD thesis, Department of Mechanical Engineering, Imperial College, University of London, Oct. 1970.

14 Hayes, D. J., and Williams, J. G., "A Practical Method for Determining Dugdale Model Solutions for Cracked Bodies of Arbitrary Shape," *International Journal of Fracture Mechanics*, Vol. 8, No. 3, pp. 239–256.

15 Dugdale, D. S., "Yielding of Steel Sheets Containing Slits," *Journal of Mechanics and Physics of Solids*, Vol. 8, 1960, pp. 100–104.

16 Swift, T., "The Effects of Fastener Flexibility and Stiffener Geometry on the Stress Intensity in Stiffened Cracked Sheet," *Proceedings of an International Conference on Prospects of Fracture Mechanics*, Delft University of Technology, The Netherlands, G. C., Sih, H. C. Van Elst, and D. Broek, Editors, June 1974, pp. 389–404.

17 Vlieger, H., "Residual Strength of Cracked Stiffened Panels," National Aerospace Laboratory, Report NLR-TR-7100 U, The Netherlands, Jan. 1971.

18 Folias, E. S., "An Axial Crack in a Pressurized Cylindrical Shell," *International Journal of Fracture Mechanics*, Vol. 1, 1965, pp. 104–108.

19 Copley, L. G., and Sanders, J. L., "A Longitudinal Crack in a Cylindrical Shell under Internal Pressure," *International Journal of Fracture Mechanics*, Vol. 5, 1969, pp. 117–131.

20 Erdogan, F., and Ratwani, M. M., "Fracture of Cylindrical and Spherical Shells Containing a Crack," *Nuclear Engineering and Design*, Vol. 20, 1972, pp. 265–286.

21 Erdogan, F., and Ratwani, M. M., "Plasticity and the Crack Opening Displacement in Shells," *International Journal of Fracture Mechanics*, Vol. 8, No. 4, 1972, pp. 413–426.

22 Anderson, R. B., and Sullivan, T. L., "Fracture Mechanics of Through-Cracked, Cylindrical Pressure Vessels," NASA TND-3252, 1966.